Properties of Pd^I–Pd^I Bonds. Theoretical and Spectroscopic Study of $Pd_2(dmb)_2X_2$ Complexes (dmb = 1,8-Diisocyano-*p*-menthane; X = Cl, Br)

Pierre D. Harvey* and Zakir Murtaza

Département de chimie, Université de Sherbrooke, Sherbrooke, Québec, Canada J1K 2R1

Received March 25, 1993®

The properties of Pd^I–Pd^I bonds and the lowest energy excited states of $Pd_2(dmb)_2X_2$ complexes (dmb = 1,8-diisocyano-*p*-menthane; X = Cl, Br) have been investigated from a theoretical and experimental point of view. M_2 σ-bonding interactions are found to arise mainly from interactions between the d_{z^2} and $d_{x^2-y^2}$ orbitals (as major components) according to extended Hückel molecular orbital calculations (EHMO), contrary to the conventional "almost pure" d_{z^2} M_2 interactions found in the prototype M–M σ-bonded compound $Mn_2(CO)_{10}$. The natures of the MO's are practically insensitive to the change in twist angle (θ; dihedral angle C–Pd–Pd–C) and to the Pd_2 bond length. The first- and second-moment analysis of the $d\sigma \rightarrow d\sigma^*$ band indicates that the excited-state distortions (ΔQ) are very large, even comparable to those of the unbridged $Mn_2(CO)_{10}$. Using the emission spectra (λ_{max} = 625 and 650 nm for X = Cl and Br, respectively) and the oxidation potentials for the first electron ($E^{0/+}$ = +0.78 and +0.064 V vs SCE for X = Cl and Br, respectively), the excited-state driving forces for electron transfer have been evaluated (1.20 and 1.27 V vs SCE for X = Cl and Br, respectively). The 77 K emission lifetimes (τ_e) range between 70 and 180 ns for the $Pd_2(diiso)_2X_2$ complexes (diiso = dmb, tmb; X = Cl, Br). Finally, according to picosecond flash photolysis observations, both photoinduced homolytic Pd_2 and PdX bond cleavages appear to be processes occurring in the $^3(d\sigma \rightarrow d\sigma^*)^*$ states of the investigated compounds. During the course of our studies, $r(Pd_2)$ values for the $Pd_2(dmb)_2X_2$ complexes (X = Cl, Br) have been evaluated to be 2.72 ± 0.05 Å on the basis of vibrational data and an empirical relationship between bond length and M_2 force constants for the closely related $Pd_2(tmb)_2Cl_2$ complex (tmb = 2,5-dimethyl-2,5-diisocyanohexane).

Introduction

Photochemical $d\sigma$, $d\sigma^*$ unbridged Pd^I–Pd^I bond homolysis has been a topic of recent interest,[1,2] including its potential applications in photoinduced palladium film deposition for defining micron-scale circuits.[3] One prototype example of a Pd^I–Pd^I bond is found in the complex $Pd_2(CNCH_3)_6^{2+}$.[1,3] The key feature is that the photogenerated $^\bullet ML_n$ radicals generally both exhibit stronger oxidant and reductant properties with respect to the ground-state metal–metal-bonded species.[3-5] One clear piece of evidence for this behavior was recently provided with the photoinduced oxidative addition reactions of the $Pd_2(diiso)_2X_2$ complexes (diiso = 1,8-diisocyano-*p*-menthane (dmb), 2,5-dimethyl-2,5-diisocyanohexane (tmb); X = Cl, Br) in the presence of CH_2Cl_2 or $CHCl_3$, where the photochemical quantum yields (Φ) were found to be large and even in one instance greater than unity.[6]

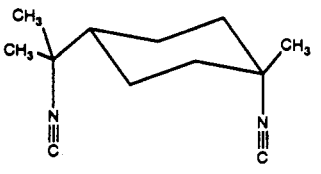

dmb

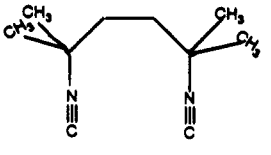

tmb

The use of bridging ligands prevents complex dissociation and may promote both metal–metal cooperation in oxidative addition reactions[7] and rapid ("energy wasting") recombination of the two photogenerated $^\bullet ML_n$ fragments. In our previous work,[6] the Φ values were found to depend upon the nature both of the bridging ligands (tmb vs dmb) and of the axially bonded halides (Cl vs Br). One interesting feature is the bite distance of the dmb ligand, which should be around 4.4 Å,[6] bridging two Pd(I) atoms that typically would exhibit in principle a bond distance of about 2.53 Å.[2] A difference of 1.9 Å between the ligand bite distance and the M_2 bond length would suggest that some stress is applied to the metal–metal bond, hence enhancing its reactivity, as previously stated.

We now wish to report our recent theoretical (EHMO), UV–vis, picosecond flash photolysis, and luminescence investigations of $Pd_2(diiso)_2X_2$ complexes (X = Cl, Br) in order to characterize the reactive Pd^I–Pd^I bonds in both the ground and excited states. A qualitative theoretical description for the MO scheme and $Pd_2L_4Cl_2$ (L = $CNCH_3$) complexes will be described, for the first time, and parameters such as ground-state metal–metal bond lengths $r(Pd_2)$ and triplet-excited-state driving forces for electron transfers will be evaluated. Using band moment analysis, it will be shown that the excited-state distortions are very large, comparable to those of the unbridged species $Mn_2(CO)_{10}$.

Experimental Section

Materials. The $Pd_2(diiso)_2X_2$ complexes[6] (diiso = tmb,[8] dmb,[8] X = Cl, Br) were prepared according to literature procedures. Ethanol and butyronitrile (Aldrich Chemical Co.) were purified by fractional distillation and dried over metallic sodium for ethanol and CaH_2 for butyronitrile until the solvents were clear glasses at 77 K. All spectroscopic measurements were performed immediately after argon bubbling–degassing of the solutions, unless stated otherwise.

Spectroscopic Measurements. The absorption spectra were recorded on a Hewlett-Packard 8452 A diode array spectrometer. The measurements of the UV–vis spectra vs temperature were performed using a

* To whom correspondence should be addressed.

® Abstract published in *Advance ACS Abstracts*, October 1, 1993.

(1) (a) Metcalf, P. A.; Kubiak, C. P. *J. Am. Chem. Soc.* **1986**, *108*, 4682. (b) Reinking, M. K.; Kullberg, M. L.; Cutler, A. R.; Kubiak, C. P. *J. Am. Chem. Soc.* **1985**, *107*, 3517.
(2) Yamamoto, Y.; Yamazaki, H. *Bull. Chem. Soc. Jpn.* *58*, 1843.
(3) Lemke, F. R.; Granger, R. M.; Morgenstern, D. A.; Kubiak, C. P. *J. Am. Chem. Soc.* **1990**, *112*, 4052.
(4) Meyer, T. J.; Caspar, J. V. *Chem. Rev.* **1985**, *85*, 187.
(5) Hepp, A. F.; Wrighton, M. S. *J. Am. Chem. Soc.* **1981**, *103*, 1258.
(6) Perreault, D.; Drouin, M.; Michel, A.; Harvey, P. D. *Inorg. Chem.* **1992**, *31*, 2740.
(7) Caspar, J. V. *J. Am. Chem. Soc.* **1985**, *107*, 6718.
(8) Weber, W. P.; Gokel, G. W.; Ugi, I. K. *Angew. Chem., Int. Ed. Engl.* **1972**, *11*, 530.

0020-1669/93/1332-4721$04.00/0

home-made assembly. The sample temperature, which was controlled by a cooled N_2(g) flow going from the bottom to the top of a cylindrical quartz Dewar cell, was monitored using a calibrated gold–chromel thermocouple (using an ice/water bath as reference temperature) and finally was allowed to stabilize for ~5 min prior to each measurement. The luminescence spectra were obtained on a steady-state LS-100 spectrofluorometer from Photon Technology Inc.

The Raman spectra were obtained on two different spectrometers. The first one was an Instruments SA Raman spectrometer equipped with a U-1000 Jobin-Yvon 1.0-m double monochromator using either the 647.1-nm red line or the 514.5-nm green line of a Spectra-Physics krypton or argon ion laser, respectively, for excitation. The second one was a Bruker IFS 66/CS FT-IR spectrometer coupled with an FRA106 FT-Raman module using a Nd:YAG laser (1064-mm excitation) and a Notch filter (cutoff ~ 70 cm^{-1}). The far-IR spectra were recorded on a FT-BOMEM DA 3.002 spectrometer with a resolution of 4 cm^{-1}, typically using from 50 to 256 scans.

Emission Lifetime Measurements. Low-temperature lifetimes (77 K) were determined using a time-correlated single-photon-counting instrument. A Quantronix 116 mode locked Nd:YAG laser operating at 9 W and 76 MHz produced a 100-ps pulse at 1064 nm. This output was frequency-doubled to 532 nm using a KTP crystal and used to excite a Coherent 700 cavity dumped dye laser producing 8-ps pulses of 594 nm radiation at 3.8 MHz. The 1064- and 594-nm outputs were mixed using a $LiIO_3$ crystal to obtain a 381-nm excitation wavelength. Samples were dissolved in a EtOH/MeOH solution and placed in a 5 mm diameter glass NMR tube, treated to three freeze–pump–thaw cycles to deaerate, and frozen to form a transparent glass. The tube was manually aligned in a dewar with flat quartz windows to excite the sample. The emission at 640 nm was passed through a Spex 1681 monochromator and collected on a Hamatsu R2809U-11 photomultiplier tube. The resulting data were processed using a multiple-exponential-fit program.

Cyclic Voltammetry Experiments. All electrochemical measurements were performed with a PAR 173 potentiostat and a PAR 175 universal programmer. Pt disk electrodes (0.5-mm diameter) were polished with alumina (5-μm size) for 5 min in 1:1 CH_3OH/H_2O before use. The cyclic voltammetric cell was a one-compartment cell (5-cm diameter) into which the working, Pt (1 cm × 1 cm) gauze auxiliary, and the reference SCE electrodes were inserted.

Picosecond Time-Resolved Measurements. The laser source for the picosecond time-resolved kinetic measurements was a mode-locked Nd:YAG laser (Quantel YG 402). Both the harmonic (532 or 355 nm) and the residual 1064-nm light pulses were extracted from the laser and traveled together to a dichroic mirror that reflected the harmonic laser pulse through a 90° angle but transmitted the 1064-nm light. While the harmonic light was focused onto the sample cuvette, the 1064-nm light traversed a variable-delay path before being focused onto a 10-cm cuvette containing a 50:50 mixture of deuteriated phosphoric acid and D_2O to produce a white continuum light flash of 30-ps duration. The continuum light was focused through a diffusing frosted glass plate and recollimated and focused onto the common end of a bifurcated fiber optics bundle that split the beam into two branches, a sample beam that probed the sample where it was excited by the harmonic laser pulse (excited state) and a reference beam that probed the sample where it was not excited (ground state). The two light beams were picked up by fiber optics on the other side of the cuvette and directed into a UFS 200 spectrograph to which a dual diode array (2 × 512) with image intensifier was attached. Thus, with one single continuum flash, the spectra of excited and unexcited samples could be detected. The wavelength resolution of the system was 1 mm per diode. The diode array data were passed via a Tracor Northern 6200 multichannel analyzer to a personal computer for storage, analysis, and display. In a typical experiment, about 200 spectra were averaged for one delay time. By moving the delay stage, the arrival of the continuum flash could be delayed by up to 5 ns with respect to the excitation pulse, thereby generating time-resolved spectra with a time resolution that was limited only by the pulse width of the laser (ca. 30 ps). Before each measurement, the two diode arrays were balanced and all reference beam data were corrected by this balance factor before calculating the difference absorption of the transient species for each wavelength: A = log (I(reference)/I(sample).

Molecular Orbital Calculations. Extended Hückel molecular orbital calculations (EHMO)[9] were performed on an IBM 486 computer using a modified version of the Wolfsberg–Helmohlz formula.[10] The atomic parameters used for C, O, H, and Cl were taken from ref 9; those for the Pd atoms were taken from ref 11. The detailed description of the graphic programs used in this work can be found in ref 12. Because of limitations in the size of the molecules handled by the program, tmb and dmb were replaced by two $CNCH_3$ groups. This procedure is standard. The Pd—C, C≡N, N—C, and Pd—Cl bond lengths have been taken as 2.00,[13] 1.14,[13] 1.45,[13] and 2.40 Å,[2] as found crystallographically for other d^9–d^9 systems ($Pd_2(CNCH_3)_6^{2+}$ [13] and $Pd_2(CNC(CH_3)_3)_4Cl_2$[2]). The Pd–Pd bond distance was set at 2.72 Å on the basis of the Raman and UV–vis findings (see text below). Some computations where r(Pd–Pd) varied from 2.53 to 2.78 Å were also performed.

Table I. Selected Raman Data for d^9–d^9 Complexes (cm^{-1})

	Raman		IR	
	$\nu(Pd_2)$	ν(PdX)	ν(PdX)	ref
$Pd_2(dmb)_2Cl_2$	174[6]	?	245	this work, 6
$Pd_2(tmb)_2Cl_2$	172[6]	240	245	this work, 6
$Pd_2(dmb)_2Br_2$	131	194		this work
$Pd_2(tmb)_2Br_2$	129	192		this work
$Pd_2(dmpm)_2Cl_2$	140	257	260	19a
$Pd_2(dmpm)_2Br_2$	123	169	175	19a
$Pd_2(dmpm)_2(OH)_2$	140	351		19a
$[Pd_2(CNCH_3)_6](PF_6)_2$	160	294		19b
$Pd_2(dppm)_2Cl_2$	152	247	273	19c
$Pd_2(dppm)_2Br_2$	120	213	189	19c

Results and Discussion

The Pd_2 Bond Length. Dipalladium complexes having strong Pd–Pd bonding interactions exhibit $r(Pd_2)$ values ranging from 2.531 to 2.8448 Å.[13–16] The X-ray crystallographic structures of the $Pd_2(diiso)_2X_2$ complexes (diiso = dmb, tmb; X = Cl, Br) are not available. For EHMO computations and bandwidth analysis in the next two sections, it was necessary that we attempt to evaluate the $r(Pd_2)$ values. We recently suggested[17] that the metal–metal bond distances (or separations) could be estimated (within a few percent of uncertainty) using reparametrized Herschbach–Laurie (H–L) relationships; $r = a + b \ln F$,[18] where r is the internuclear distance (in Å) and F is the force constant (in mdyn $Å^{-1}$). For Pd systems, the H–L equation is[17b]

$$r(Pd_2) = -0.387 \ln F(Pd_2) + 2.67 \qquad (1)$$

with a correlation coefficient (σ) of 0.99, using 12 data points.

In these cases, the largest deviation from the line of 0.05 Å, for which the relationship fits $r(Pd_2)$ experimental values, ranging from 2.591 to 4.42 Å.[17b] The $\nu(Pd_2)$ values for the $Pd_2(diiso)_2Cl_2$ complexes (diiso = tmb, dmb) were already identified on the basis of the resonance Raman observation.[6] We have recorded the Raman spectra for the Br derivatives and made assignments for ν(PdX) on the basis of the literature comparison (Table I).[14,19] Typical examples of vibrational spectra are provided in Figure 1. Using the data for $Pd_2(tmb)_2Cl_2$ and the equation relating force constants and frequencies for X–M–M–X systems[20] (λ_1 +

(9) (a) Hoffmann, R.; Lipscomb, W. N. *J. Chem. Phys.* **1962**, *86*, 2179. (b) Hoffmann, R.; Lipscomb, W. N. *J. Chem. Phys.* *37*, 2872. (c) Hoffman, R. *J. Chem. Phys.* **1963**, *39*, 1392.

(10) Ammeter, J. H.; Burgi, H. B.; Thibeault, J. C.; Hoffmann, R. *J. Am. Chem. Soc.* **1978**, *100*, 3686.

(11) Tatsumi, K.; Hoffmann, R.; Yamamoto, A.; Stilke, T. K. *Bull. Chem. Soc. Jpn.* **1981**, *54*, 1857.

(12) Mealli, C.; Proserpio, D. M. *J. Chem. Educ.* **1990**, *67*, 399.

(13) Goldberg, S. Z.; Eisenberg, R. *Inorg. Chem.* **1976**, *15*, 535.

(14) (a) Kullberg, M. L.; Lemke, F. R.; Powell, D. R.; Kubiak, C. P. *Inorg. Chem.* **1985**, *24*, 3589. (b) Colton, R.; McCornick, M. J.; Pannan, C. D. *Aust. J. Chem.* **1978**, *31*, 1425.

(15) Rutherford, N. M.; Olmstead, M. M.; Balch, A. L. *Inorg. Chem.* **1984**, *23*, 2833.

(16) For recent examples, see: (a) Kraft, T. E.; Hejna, C. I.; Smith, J. S. *Inorg. Chem.* **1990**, *29*, 2682 and references therein. (b) Wilson, W. L.; Nelson, J. H. *Organometallics* **1990**, *9*, 1699. (c) Micklitz, W.; Sheldrick, W. S.; Lippert, B. *Inorg. Chem.* **1990**, *29*, 211.

(17) (a) Perreault, D.; Drouin, M.; Michel, A.; Miskowski, V. M.; Schaefer, W. P.; Harvey, P. D. *Inorg. Chem.* **1992**, *31*, 695. (b) Perreault, D.; Drouin, M.; Michel, A.; Harvey, P. D. *Inorg. Chem.* **1993**, *32*, 1903.

(18) Hershbach, D. R.; Laurie, V. W. *J. Chem. Phys.* **1961**, *35*, 458.

(19) (a) Kullberg, M. L.; Lemke, F. R.; Powell, D. R.; Kubiak, C. P. *Inorg. Chem.* **1985**, *24*, 3589. (b) Clark, R. J. H.; Sourisseau, C. *Nouv. J. Chim.* **1980**, *4*, 287. (c) Alvers, O. L.; Virtoge, M.-C.; Sourisseau, C. *Nouv. J. Chim.* **1983**, *7*, 231.

Table II. Atomic Orbital Contributions for the $Pd_2(CNCH_3)_4Cl_2$ Molecular Orbitals: Top for $\theta = 90°$ and $r = 2.53$ Å; Bottom for $\theta = 0°$, $r = 2.72$ Å, and "bite distance" (r(C···C)) = 4.0 Å

MO no.	% Pd orbitals							% Cl- (p_z)	% C- (p_x or p_y)	EHMO energy/eV	MO description
	p_z	s	d_{z^2}	$d_{x^2-y^2}$	d_{xy}	d_{xz}	d_{yz}				
37		4	52	22				4	12	−9.581	dσ*(LUMO)[a]
38	6	12	18	50				4		−11.197	dσ(HOMO)[a]
39						96				−11.756	dπ*
40							96			−11.756	dπ*
41		4	34	60						−11.769	mixed "dσ*, dσ*"
42					96					−12.027	dδ*
43			62	32				4		−12.055	mixed "dσ, dδ"
44					94					−12.090	dδ
45						93				−12.180	dπ
46							93			−12.180	dπ

MO no.	• % Pd orbitals							% Cl- (p_z)	% C- (p_x or p_y)	EHMO energy/eV	MO description
	p_z	s	d_{z^2}	$d_{x^2-y^2}$	d_{xy}	d_{xz}	d_{yz}				
37		6	46	20				10	12	−9.451	dσ*(LUMO)[a]
38	6	18	22	32				8	8	−10.585	dσ(HOMO)[a]
39							82			−11.417	dπ*
40		4	36	60						−11.788	mixed "dσ*, dσ*"
41							80			−11.804	dπ
42						98				−11.833	dπ*
43			50	46						−12.009	mixed "dδ, dσ"
44					92					−12.051	dδ*
45					92					−12.084	dδ
46						98				−12.103	dπ

[a] Note that these MO's are mixed dσ, dδ (HOMO) or dσ*, dδ* (LUMO); see text.

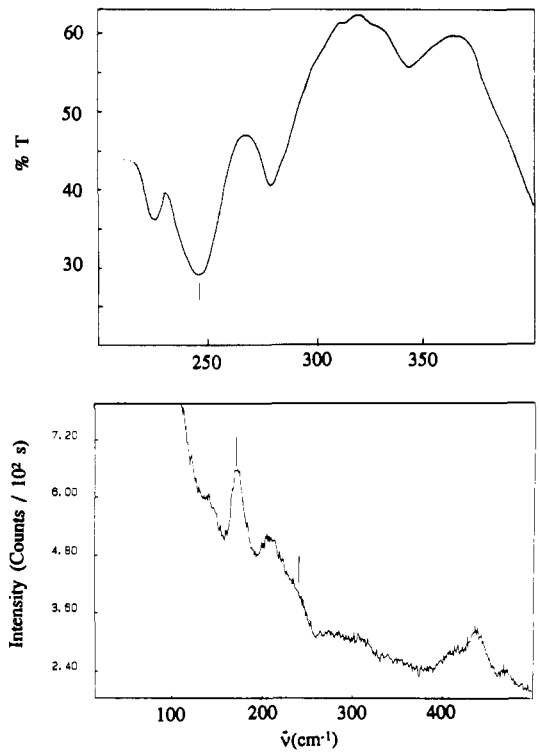

Figure 1. Far-IR and Raman spectra of solid $Pd_2(tmb)_2Cl_2$. Experimental conditions: far-IR, 300 scans, resolutio 4 cm^{-1}; Raman, λ_{exc} = 632 nm, 32 × objective, 1 s/point, 1 point/cm^{-1}. The marked peaks are the peaks of interest in this work.

$\lambda_2 - \lambda_3 = F(M_2)/\mu$, where $\lambda_i = (2\pi c\nu_i)^2$, μ = reduced mass, $\nu_1 = \nu(Pd_2)$, $\nu_2 = \nu(PdX)_{sym}$, and $\nu_3 = \nu(PdX)_{asym}$), a value of 0.87 mdyn $Å^{-1}$ is obtained for $F(Pd_2)$. For such an F value, eq 1 gives a distance of 2.72 Å, which compares favorably with some known values for bridged d^9–d^9 species ($Pd_2(dppm)_2Br_2$ ($r(Pd_2)$ = 2.699 Å;[21] $Pd_2(\mu\text{-}CO)_2Cl_4)^{2-}$ ($r(Pd_2)$ = 2.697 Å)[22] and is relatively close to the internuclear distance found in palladium metal (2.751 Å).[23] The uncertainty is ±0.05 Å (as stated above) and is reasonable for the purpose of this work.

We have not been able to obtain $\nu(PdCl)_{sym}$ for $Pd_2(dmb)_2Cl_2$ due to the high laser sensitivity of the compound; only (low power) resonance-enhanced bands were observed (e.g. $\nu(Pd_2)$) in this case.[6] Due to the fact that both $\nu(Pd_2)$ and $\nu(PdCl)_{asym}$ are about the same, it is assumed that $\nu(PdCl)_{sym}$ is also the same, placing $r(Pd_2)$ at ~2.72 Å. For the bromide derivatives, $r(Pd_2)$ can also be reasonably set at the same value, since the $r(Pd_2)$ is nearly independent of the axial ligand for the same family of compounds (for example: $Pd_2(CNCH_3)_6^{2+}$ (2.531 Å);[13] $Pd_2(CNC(CH_3)_3)_4Cl_2$ (2.532 Å);[2] $Pd_2(CNCH_3)_4I_2$ (2.533 Å);[15] $Pd_2(CN\text{-}2,6\text{-}(C(CH_3)_3)_2\text{-}4\text{-}(CH_3)C_6H_2)_4Cl_2$ (2.562 Å)).[24a] Such behavior has also been noted for a wide range of dinuclear platinum(III) complexes with the basic structure $Pt_2(POP)_4L_2^{4-}$ (POP = $P_2O_5H_2^{2-}$), with $2.70 > r(Pt_2) < 2.76$ Å.[24b,c]

EHMO Computations. We have performed extended Hückel molecular orbital calculations (EHMO) in order to obtain some qualitative information on the nature of the HOMO and LUMO and the MO dependence (particularly for the dσ → dσ* transition energy) upon the metal–metal distance ($r(Pd_2)$) and on the twist angle between the $Pd(L)_2X$ planes (X = Cl; L = $CNCH_3$; θ = twist angle). Only brief (and superficial) MO schemes of some selected d^9–d^9 species have been reported in the literature.[25] A description of the molecular orbitals for the model compound $Pd_2(CNCH_3)_4Cl_2$ appears appropriate at this time. The internuclear distances used for the computations are those for $Pd_2(CNC(CH_3)_3)_4Cl_2$[2] using $\theta = 90°$ (D_{2d} local symmetry). Table II summarizes the results, and Figure 2 shows the interaction diagram for the two $Pd(CNCH_3)_2Cl$ fragments. The coordinate

(20) Herzberg, G. *Molecular Spectra and Molecular Structure*; Van Nostrand: New York, 1945; Vol. II, p 180.
(21) Holloway, R. G.; Penhold, B. R.; Colton, R.; McCormick, M. J. *J. Chem. Soc., Chem. Commun.* **1976**, 485.
(22) Wagner, D. P.; Hess, R. W.; Treichel, P. M.; Calabrese, J. C. *Inorg. Chem.* **1975**, *14*, 1121.
(23) Donohue, J. *The Structure of the Elements*; Wiley: New York, 1974; p 216.
(24) (a) Yamamoto, Y.; Y.; Takahashi, K.; Yamazaki, H. *Chem. Lett.* **1985**, 201. (b) Che, C.-M.; Lee, W.-M.; Mak, T. C. W.; Gray, H. B. *J. Am. Chem. Soc.* **1986**, *108*, 4446. (c) Alexander, K. A.; Bryan, S. A.; Fronczek, F. R.; Fultz, W. C.; Rheingold, A. L.; Roundhill, D. M.; Stein, P.; Watkins, S. F. *Inorg. Chem.* **1985**, *24*, 2803.
(25) (a) Zeitlow-Heinrich, M. Ph.D. Thesis, California Institute of Technology, 1988. (b) Kostic, N. M.; Fenske, R. F. *Inorg. Chem.* **1983**, *22*, 666. (c) Albright, T. A.; Burdett, J. K.; Whangbo, M.-H. *Orbitals Interactions in Chemistry*; Wiley: New York, 1984; pp 340, 354. (d) Hoffman, D. M.; Hoffman, R. *Inorg. Chem.* **1981**, *20*, 3543. (e) Yip, H. K.; Che, C.-M.; Peng, S. M. *J. Chem. Soc., Dalton Trans.* **1993**, 179.

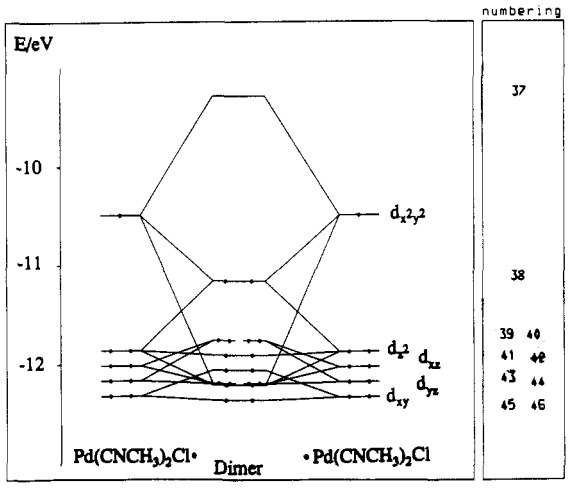

Figure 2. Interaction diagram of two $Pd(CNCH_3)_2Cl$ fragments with a 90° twist angle. In the dimer, the $r(Pd_2)$ value is set at 2.53 Å.

system used for the local set of axes of each ML_3 fragments are the z axis placed perpendicular to the planes and the y axis placed along the L–M–L axis. This coordinate system is used in the description of the results in Table II and III. The most interesting features are the atomic contributions for the LUMO (b_2) and HOMO (a_1), where both d_{z^2} and $d_{x^2-y^2}$ orbitals contribute significantly to the $d\sigma^*$ (52% and 22%) and $d\sigma$ (18% and 50%) orbitals, respectively. It is also noted that some "s" and "p_z" character is seen in the MO contributions. The observed MO shapes for the HOMO and LUMO are a result of "adding" and "canceling" effects of the atomic orbitals. The adding effect arises between two orbitals of the same sign while the negative (destructive) effect takes place between two orbitals of opposite signs. In principle, the addition of d_{z^2} and $d_{x^2-y^2}$ (in equal amounts) would generate an octahedral-shaped MO. This is obviously not the case (Figure 3). Table III provides the detailed atomic contributions (including the sign) for the LUMO and HOMO, which explain the observed shapes.

This situation is unique for a description of an M_2 σ-bond. It has long been known that, commonly, the M_2 σ-bonding arises almost entirely from d_{z^2}–d_{z^2} orbital overlaps.[26] This difference derives from a geometric situation where two square planar metal complexes interact not in a face-to-face fashion but rather via a side-by-side one where two ML_3 fragments share a common side. The M_2 σ-bonding is best described by a mix of both forms of interactions, namely d_{z^2}–3_{z^2} (side-by-side, form I) and $d_{x^2-y^2}$–$d_{x^2-y^2}$

I II

(form II). However, it is important to realize that the d_{x^2}–d_{z^2} side-by-side interactions are not significant (with respect to the $d_{x^2-y^2}$ ones) and that the bonding nature of the Pd–Pd bond is created mainly by the interactions between the $d_{x^2-y^2}$ and $d_{x^2-y^2}$ orbitals.

As expected, the LUMO and HOMO exhibit some significant ligand atomic orbitals contributions which originate from the M–L interactions in the ML_3 fragments.[25c] In both cases, the M–L interactions are antibonding (Figure 3), indicating that the excited-state distortions (ΔQ) for the Pd–Cl and Pd–C bonds are not expected to be too large in the $^{1,3}(d\sigma \rightarrow d\sigma^*)^*$ ($^{1,3}B_2$) excited states.

Two other orbitals (numbers 41 and 43) experience the same fate as orbitals for the LUMO and the HOMO, where the atomic contributions are 34% and 60% for MO 41 and 62% and 32% for

(26) Levenson, R. Ph.D. Thesis, Columbia University, 1970.

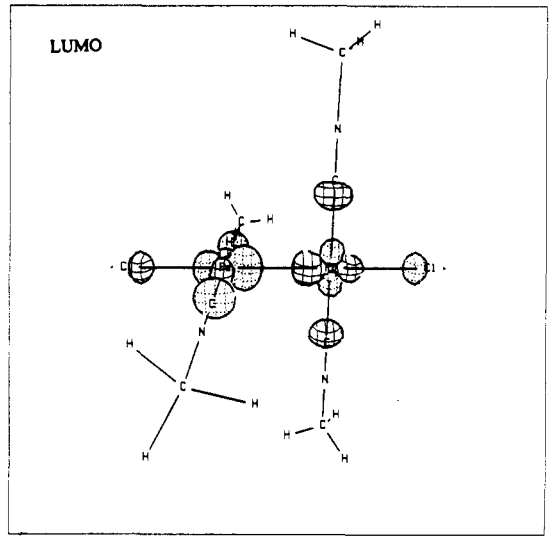

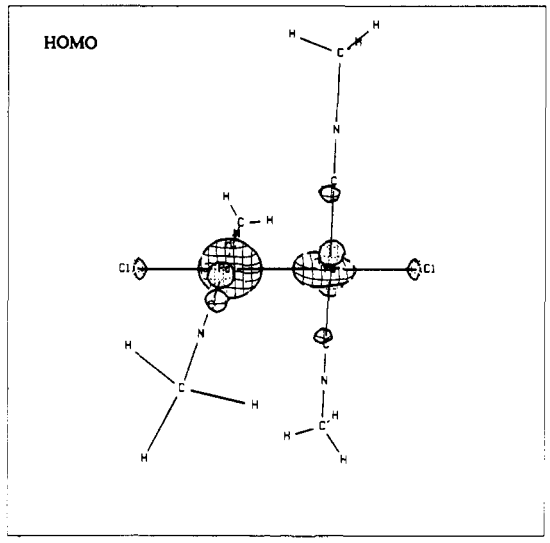

Figure 3. Diagrams of the b_2(LUMO) and a_1(HOMO) orbitals for the compound $Pd_2(CNCH_3)_4Cl_2$. $\theta = 90°$; $r(Pd_2) = 2.53$ Å (D_{2d} point group).

Table III. Detailed HOMO and LUMO Analysis[a]

LUMO			HOMO		
atomic orbital	contribn/%	sign	atomic orbital	contribution	sign
Pd s	6	+	Pd s	3%	–
Pd p_z	3	+	$d_{x^2-y^2}$	11%	+
Pd $d_{x^2-y^2}$	25	–	Pd d_{z^2}	26%	–
Pd d_{z^2}	8	+	Cl p_y	3%	+
Cl p_y	2	–	C p_x	2%	+
Pd s	7	+	C p_y	2%	–
Pd p_z	3	–	Pd s	3%	+
Pd $d_{x^2-y^2}$	25	+	Pd $d_{x^2-y^2}$	11%	+
Pd d_{z^2}	8	+	Pd d_{z^2}	26%	+
Cl p_x	2	+	p_x	3%	+
			C p_y	2%	–
			C p_x	2%	+

[a] The axis labels are those of a local set of axes at the metal center where the "z" axis is perpendicular to each ML_3 plane.

MO 43 for the d_{z^2} and $d_{x^2-y^2}$ Pd orbitals, respectively. This result implies that these four MO's are mixed in nature, i.e., $d\sigma$ and $d\delta$. The MO diagrams for the HOMO and LUMO's are shown in Figure 3, in which the σ-bonding interactions differ slightly from what has been predicted.[25,26] It is also interesting to note that the computed energy gaps between the HOMO and the HOMO-1 and HOMO-2 are 4510 and 5720 cm^{-1}, respectively, which compare favorably with the energy gaps between the lowest energy band ($d\sigma \rightarrow d\sigma^*$; 307 nm = 32 600 cm^{-1}) and the higher ones located at ~ 271 nm (36 900 cm^{-1}; shoulder) and 258 nm (38 800 cm^{-1}), respectively, reported for $Pd_2(CNC(CH_3)_3)_4Cl_2$.[2]

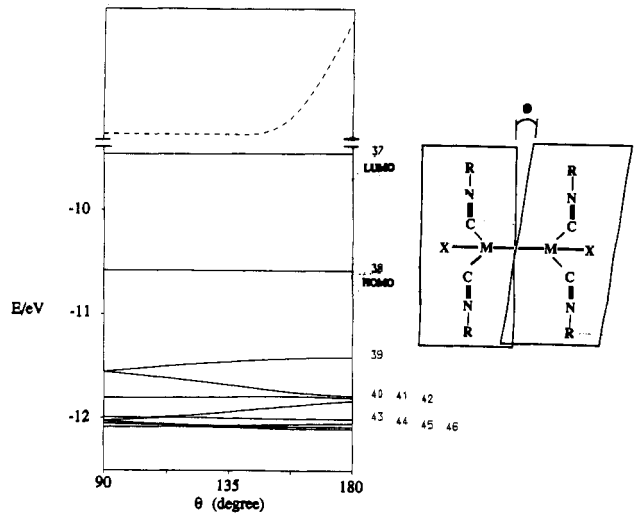

Figure 4. Left: Walsh diagram of the MO energies for the model compound $Pd_2(CNCH_3)_4Cl_2$ as a function of the twist angle θ ($D_{2d} \rightarrow D_2 \rightarrow D_{2h}$) with $r(Pd_2)$ = 2.72 Å. Right: EHMO total energy as a function of θ (the minimum and maximum energy difference is ~ 0.1 eV).

For the bridged species investigated in this work, it appears very unlikely that θ = 90 or 0°. The bite distances for the tmb and dmb ligands are around 3.3[27] and 4.4 Å,[6,28] respectively (distances at which the M atoms are interacting very weakly). Previous X-ray crystallographic work for Rh_2 and Ir_2 complexes[29-31] has shown that the dmb ligand is capable of bridging M_2 bonds of 2.99 and 3.16 Å,[29] up to M···M distances of ~5.2 Å.[30] To accommodate such variation in distance (with respect to the reference value of 4.4 Å), large deviations of the twist angle (θ)[29b] and bond angle distortions (C–M–C; M = Rh, ∠ = 169.7(3)°)[29a] have been noted. Large distortions are also expected for the $Pd_2(dmb)_2X_2$ complexes (X = Cl, Br; $r(Pd_2)$ ~ 2.72 Å). The plot of the computed EHMO energies vs θ (Walsh diagram; Figure 4) for $Pd_2(CNCH_3)_4Cl_2$ (with $r(Pd_2)$ = 2.72 Å and bite distance = 4.0 Å at θ = 0°) shows that the energies of the HOMO and LUMO's are rigorously θ independent. On the other hand, the lower energy MO's are θ dependent. The EHMO total energy does not vary between 90 and ~145° but increases between 145 and 180° (Figure 4). This increase in energy in these models is not related to steric interactions between the CH_3NC ligands but rather is purely electronic in origin. This energy difference is somewhat small: ~800 cm^{-1} for $r(Pd_2)$ = 2.72 Å. The θ values reported for $Pd_2(dppm)_2X_2$ (X = Cl, I, O_2CCF_3; dppm = $((C_6H_5)_2P)_2CH_2$) vary from 39 to 45°, respectively.[31] Knowing that the dppm bite distance is ~3 Å,[32,33] which is close to the Pd_2 bond length (~2.7 Å), we assume these relatively large dihedral angles to be a consequence of both ligand geometrical (major) and Pd electronic (minor) factors. This conclusion is consistent with the cylindrical nature of the σ-bonding.

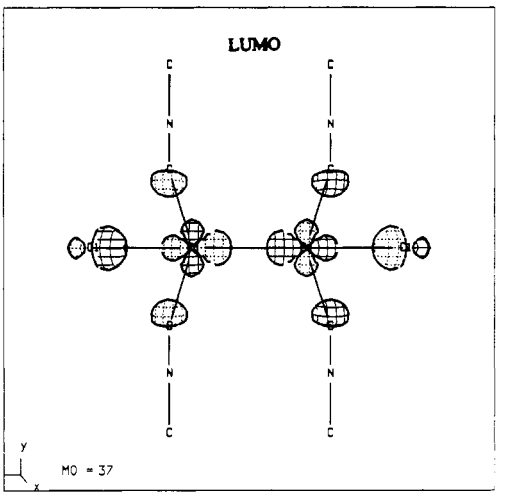

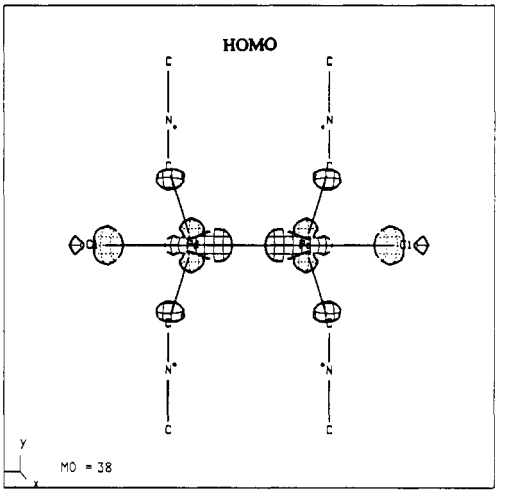

Figure 5. Diagrams of the b_{1u}(LUMO) and a_{1g}(HOMO) orbitals for the compound $Pd_2(CNCH_3)_4Cl_2$. θ = 180°; $r(Pd_2)$ = 2.72 Å; C···C = 4.0 Å (D_{2h} point group).

It is also interesting to note that the MO's do not greatly vary in nature with what has been described for $Pd_2(CNCH_3)_4Cl_2$ (θ = 90°, $r(Pd_2)$ = 2.53 Å). Table II summarizes the atomic contributions for $Pd_2(CNCH_3)_4Cl_2$ with θ = 0° (D_{2h} local symmetry), $r(Pd_2)$ = 2.72 Å, and the C···C distance kept at 4.0 Å. The slight changes in MO ordering are simply due to the change in θ (see the Walsh diagram in Figure 4), combined with the change in $r(Pd_2)$ (see text below). Diagrams of the LUMO (b_{1u}) and HOMO (a_{1g}) for the $Pd_2(CNCH_3)_4Cl_2$ compound, where θ = 0° (D_{2h} local symmetry), are shown in Figure 5. These pictures exhibit many similarities with those shown in Figure 3.

The EHMO energy dependence upon $r(Pd_2)$ between 2.54 and 2.78 Å (reasonable limits for a Pd^I–Pd^I single bond), where the bite distance is kept constant at 4.0 Å and θ = 0°, behaves as expected; the HOMO–LUMO energy gap decreases with $r(Pd_2)$ (Figure 6). A comparison of literature data (Table IV)[2,13,19,34-37] allows confirmation of this trend. Interestingly, the estimated 2.72 Å values for $r(Pd_2)$ for the diisocyano complexes (vs λ_{max} ($d\sigma \rightarrow d\sigma^*$)) are consistent with the literature data.[2,13,19,34-37]

One more comment should be added concerning MO 39 ($d\pi^*$), which undergoes sensitive EHMO stabilization upon the increase

(27) Mann, K. R.; Thick, J. A.; Bell, R. A.; Coyle, C. A.; Gray, H. B. *Inorg. Chem.* **1980**, *19*, 2462.
(28) Che, C.-M.; Herbstein, F. H.; Schaefer, W. P.; Marsh, R. E.; Gray, H. B. *Inorg. Chem.* **1984**, *23*, 2572.
(29) (a) Boyd, D. C.; Matsch, P. A.; Mixa, M. M.; Mann, K. R. *Inorg. Chem.* **1986**, *25*, 3331. (b) Sykes, A. G.; Mann, K. R. *J. Am. Chem. Soc.* **1990**, *112*, 7247.
(30) Sykes, A.; Mann, K. R. *J. Am. Chem. Soc.* **1988**, *110*, 8252.
(31) (a) Colton, R.; McCormick, J. M.; Pannan, D. C. *Aust. J. Chem.* **1978**, *31*, 1425. (b) Krafft, T. E.; Hejna, C. I.; Smith, J. S. *Inorg. Chem.* **19910**, *29*, 2682. (c) We have used the commercially available PC-MODEL program to obtain the "minimized" structure of a model compound $Pd_2(H)_4(C_{14}H_{18})_2Cl_2$. The PC-MODEL program does not perform calculations for square planar structures and strongly distorts the isocyanide angles (due to the tetravalent nitrogen assumed to be N^+). Instead we have replaced N^+ by C in the dmb ligands and added four nonsterically demanding H atoms to complete the *octahedral* structure of the Pd atoms. The computed dihedral angles (CPdPdC) are 53.4°. The computed bond length distances (PdC and PdCl) compare favorably to the ones observed by X-ray crystallography for the other d^9–d^9 species (see text). A figure for the structure is provided in the supplementary material.
(32) Manojlovic-Muir, L. J.; Muir, K. W.; Grossel, M. C.; Brown, M. P.; Nelson, C. P.; Yavari, A.; Kallas, E.; Moulding, R. P.; Seddon, K. R. *J. Chem. Soc., Dalton Trans.* **1986**, 1955.
(33) Kirss, R. V.; Eisenberg, R. *Inorg. Chem.* **1989**, *28*, 3372.
(34) Olmstead, M. M.; Benner, L. S.; Hope, H.; Balch, A. L. *Inorg. Chim. Acta* **1979**, *32*, 193.
(35) Yamamoto, Y.; Yamazaki, H. *Inorg. Chem.* **1986**, *25*, 3327.
(36) Yamamoto, Y.; Takahashi, K.; Yamazaki, H. *Chem. Lett.* **1985**, 201.
(37) Retig, M. F.; Kirk, E. A.; Maitlis, P. M. *J. Organomet. Chem.* **1976**, *111*, 113.

Table IV. Spectroscopic and Structural Data for d^9–d^9 Complexes

complex	$r(Pd_2)$/Å	$\lambda_{max}(d\sigma \rightarrow d\sigma^*)$/nm	$\nu_{max}(d\sigma \rightarrow d\sigma^*)$/cm^{-1}	ref
$Pd_2(dmb)_2Cl_2$	~2.72[a]	438[b]	22 800	this work
$Pd_2(dmb)_2Br_2$	~2.72[a]	422[b]	23 700	this work
$Pd_2(dppm)_2Br_2$	2.699	426	23 500	19c, 21
$Pd_2(dppm)_2(Cl)(SnCl_3)$	2.644	420[c]	23 810	19c, 34
$Pd_2(2,6\text{-}(CH_3)_2C_6H_3NC)_2(Py)_2$	2.662	377	26 500	35
$Pd_2(dmpm)_2Br_2$	2.603	394	25 400	19a
$Pd_2(2,6\text{-}((CH_3)_3C)_2\text{-}4\text{-}CH_3C_6H_2NC)_4Cl_2$	2.562	324	30 900	36
$Pd(CNC(CH_3)_3)_4Cl_2$	2.532	307	32 600	2
$Pd_2(CNCH_3)_6^{2+}$	2.531	302	33 100	13, 37

[a] See text. [b] Ethanol solutions. [c] The lowest energy band is located at 493 nm (17 000 M^{-1} cm^{-1}) but was assigned to a charge-transfer band.[19c] We assign the next band to $d\sigma \rightarrow d\sigma^*$ on the basis of the appropriate energy and absorptivity.

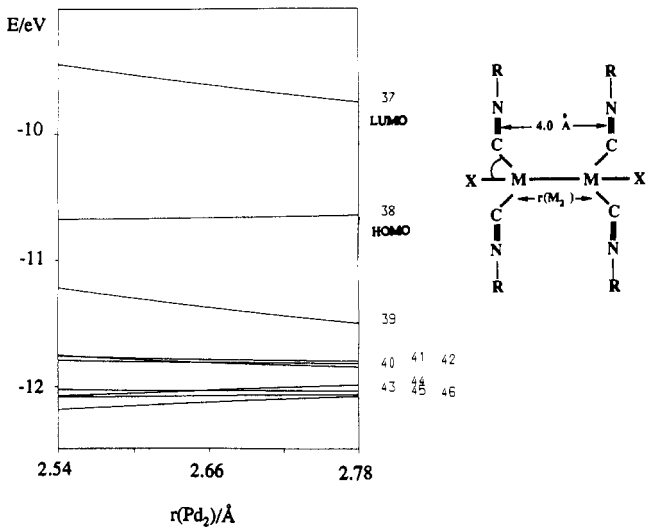

Figure 6. Walsh diagram of the MO energies for the model compound $Pd_2(CNCH_3)_4Cl_2$ as a function of $r(Pd_2)$ from 2.54 to 2.78 Å with a "bite distance" (C···C distance) kept constant at 4.0 Å.

of $r(Pd_2)$ (Figure 6). Mainly composed of the in-plane d_{yz} Pd orbitals (82%), this molecular orbitals has an antibonding nature and favors Pd–Pd dissociation. Consequently, the decrease in MO energy with $r(Pd_2)$ appears to contribute (relatively) strongly to the relative bond lengthening of $r(Pd_2)$ observed in these systems ($r(Pd_2)$ = 2.72 ± 0.05 Å) in comparison with the unbridged systems ($Pd_2(CNC(CH_3)_3)_4Cl_2$; $r(Pd_2)$ = 2.53 Å). Unfortunately, the EHMO methods are poor when minimum energy distances are concerned; it is not theoretically possible to predict the M–M distance in this case.

UV–Visible Frequencies vs Temperature. During the course of our studies, we have noticed that both λ_{max} and bandwidth of the lowest energy bands ($d\sigma \rightarrow d\sigma^*$) experience remarkable decreases with temperature (Figure 7). This drastic thermal behavior is known to be characteristic of metal–metal $d\sigma \rightarrow d\sigma^*$ transitions[38] and is attributed[38a] to the important Franck–Condon terms that the electronic transition should exhibit for relatively low-frequency modes; i.e. $\nu(M_2)$. Miskowski *et al.*[38a] have used moment analysis[39] to quantify the temperature effect on the $d\sigma \rightarrow d\sigma^*$ band for some d^7–d^7 Rh_2 complexes and $Mn_2(CO)_{10}$. We have followed the same approach in this work. For an allowed transition,[40] the oscillator strength is temperature independent. The normalized first and second moments (parameters of interest

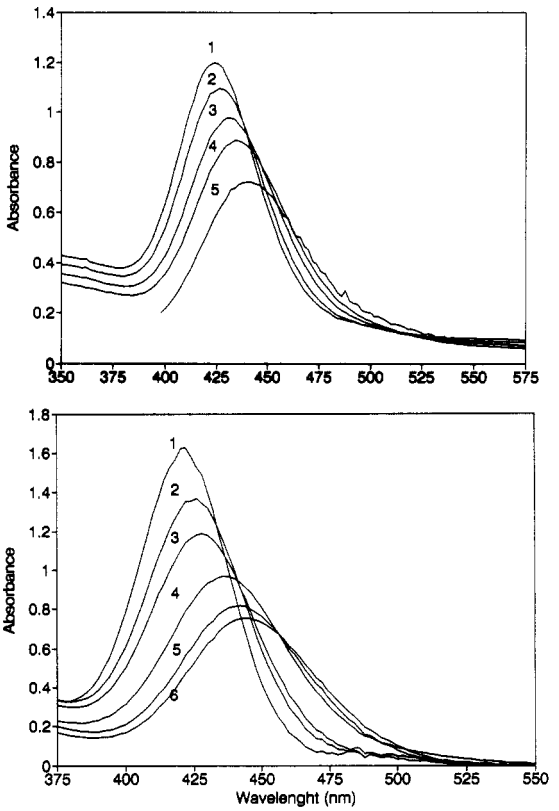

Figure 7. (Selected) UV–vis spectra of the $Pd_2(dmb)_2X_2$ complexes in ethanol as a function of temperature. X = Cl, top: 1 = 105 K, 2 = 150 K, 3 = 180 K, 4 = 220 K, 5 = 300 K. X = Br, bottom: 1 = 80 K, 2 = 135 K, 3 = 190 K, 4 = 240 K, 5 = 280 K, 6 = 300 K.

in this analysis) and $\bar{\nu}_{max}$ and m^2 ($(8 \ln 2)^{-1}$(fwhm)^2; fwhm = full width at half-maximum) when the band is Gaussian shaped (which is a good approximation in this work).

When the ground-state vibrational modes (involved in the Franck–Condon terms) are harmonic oscillators (which is often the case for low-frequency modes), both $\bar{\nu}_{max}$ and m^2 follow a temperature dependence of the form

$$\bar{\nu}_{max} \text{ and } m^2 = \sum_i A_i \coth\left(\frac{\hbar\omega_i}{2kT}\right) + B \qquad (2)$$

where k = Boltzmann constant, T = temperature, and $\hbar\omega_i$ are the ground-state vibrational frequencies (for an absorption spectrum). The temperature-independent B term in the first-moment equation is related to the electronic transition energy. The B value for the second moment should be either zero or very small, according to theory.[39] For non-zero B values, it has been proposed[38a] that they be attributed to Franck–Condon-active modes that are too energetic to contribute strongly to the temperature dependence. Such modes could be the Raman active ν(M–L), according to Miskowski *et al.*[38a]

In order to test such an analysis, we have looked at the second moments at two temperatures for $Pd_2(dppm)_3$,[32] a related

(38) (a) Miskowski, V. M.; Smith, T. P.; Loehr, T. M.; Gray, H. B. *J. Am. Chem. Soc.* **1985**, *107*, 7925. (b) Levenson, R. A.; Gray, H. B. *J. Am. Chem. Soc.* **1975**, *97*, 6042. (c) Wrighton, M. S.; Ginley, D. S. *J. Am. Chem. Soc.* **1975**, *97*, 4246. (d) Abrahamson, H. B.; Frazier, C. C.; Ginley, D. S.; Gray, H. B.; Lilienthal, J.; Tyler, D. R.; Wrighton, M. S. *Inorg. Chem.* **1977**, *16*, 1554. (e) Tyler, D. R.; Levenson, R. A.; Gray, H. B. *J. Am. Chem. Soc.* **1978**, *100*, 7888.

(39) (a) Markham, J. J. *Rev. Mod. Phys.* **1959**, *31*, 956. (b) Ballhausen, C. J. *Molecular Electronic Structures of Transition Metal Complexes*; McGraw-Hill: New York, 1979; pp 132–135.

(40) Absorptivity data[6] for the $d\sigma \rightarrow d\sigma^*$ bands (in aceonitrile solutions): $Pd_2(dmb)_2Cl_2$, 448 nm (9070 M^{-1} cm^{-1}); $Pd_2(dmb)_2Br_2$, 446 nm (6290 M^{-1} cm^{-1}).

Table V. Best-Fit First-Moment ($\bar{\nu}_{max}$) and Second-Moment (m^2) Parameters

	1st moment best fit/cm^{-1}			2nd moment best fit/cm^{-2}	
	$\hbar\omega_i$	A	B	A^a	B^a
$Pd_2(dmb)_2Cl_2$/EtOH	175 ± 15	−607	25 400	6.45×10^5	1.59×10^5
$Pd_2(dmb)_2Br_2$/EtOH	120 ± 10	−518	24 390	2.71×10^5	6.49×10^4

[a] Note that the A and B values are extracted from the graph $(fwhm)^2$ vs $\coth(\hbar\omega_i/2kT)$, where the slope and the intercept have been divided by 8 ln 2.

binuclear compound in which there is no axial ligand and for which fwhm values at 77 and 293 K are available.[41] Assuming that $B = 0$ in this case, eq 2 becomes

$$(\text{fwhm})^2 = (8 \ln 2)\sum A_i \coth\left(\frac{\hbar\omega_i}{2kT}\right) \qquad (3)$$

According to theory,[39] $A = S(\hbar\omega_e)^2$, where S is the Huang–Rhys parameter,[42] and $\hbar\omega_e$ is the excited-state frequency. Knowing that the S value is given by[39]

$$S = \left(\frac{\mu\omega_e^2}{2\hbar\omega_g}\right)(\Delta Q)^2 \qquad (4)$$

where μ is the reduced mass, $\hbar\omega_g$ is the ground-state vibrational frequency, and ΔQ is the excited-state distortion, we reformulate eq 3 as

$$\text{fwhm} = 4\pi(\Delta Q)\sum \nu_e^2 \sqrt{(\ln 2)\coth\left(\frac{0.72\nu_g}{T}\right)\frac{\mu c}{h\nu_g}} \qquad (5)$$

where ν_g and ν_e, respectively, are the vibrational frequencies in the ground and excited states, given in cm^{-1} units, and c is the speed of light. The fwhm values for $Pd_2(dppm)_3$ are 1590 and 2750 cm^{-1} at 77 and 293 K, respectively (in 2-methyltetrahydrofuran glass).[41] Using 2.96 Å for $r(Pd_2)$ in the ground state[32b] and eq 1 to obtain $r(Pd_2)$ in the excited state (from $F(Pd_2) = \mu(2\pi c\nu(Pd_2))^2$), reasonable ΔQ and S values of 0.26 and 0.27 and of 16 and 17 for $T = 77$ and 293 K, respectively, are extracted from eqs 4 and 5. The closeness of these values indicates that the assumption for B to be negligible is adequate in this case. The $\hbar\omega(Pd_2)$ in the lowest energy, triplet excited state has previously been measured (150 cm^{-1}) by time-resolved resonance Raman spectroscopy.[41b] Equation 1 gives a value of 2.80 Å for $r(Pd_2)$ in the triplet state and 2.98 Å for $r(Pd_2)$ in the ground state ($\hbar\omega(Pd_2) = 120$ cm^{-1} in the ground state).[41] The approximated ΔQ value (~0.18 Å) for the triplet state compares reasonably favorably with the one calculated for the singlet state, using moment analysis (~0.26–0.27 Å).[43]

The plots of $\bar{\nu}_{max}$ ($d\sigma \rightarrow d\sigma^*$) vs T and $(fwhm)^2$ vs $\coth(\hbar\omega 2kT)$ for the $Pd_2(dmb)_2X_2$ complexes (X = Cl, Br) are shown in Figure 8 and 9, respectively. The nonlinear least-squares best fits for the first-moment analysis are presented in Table V. The negative A values indicate a decrease in force constants between the ground and excited states, which is consistent with the decrease in bond order (1 → 0) in the excited state. The fits assume a single active vibrational mode, and adequate fits to eq 2 cannot be obtained for $\nu(M_2)$ greater than ±10%. It appears reasonable to conclude that $\hbar\omega(Pd_2)$ is the thermally important Franck–Condon-active mode.

The A values obtained for the second-moment analysis (Table IV) compare favorably to those reported for $Rh_2b_4Cl_2^{2+}$ (b = $CN(CH_2)_3NC$), $Rh_2(TMB)_4Cl_2^{2+}$, and $Mn_2(CO)_{10}$ (3.39×10^5, 3.34×10^5, and 6.10×10^5 cm^2, respectively).[38a] The large A values simply indicate that the excited-state distortions are great. Using eq 4 and the relation $A = S(\hbar\omega_e)^2$, a tabulation of ΔQ vs $\hbar\omega_e(Pd_2)$ is obtained (Table VI). Both ΔQ and $\hbar\omega_e(Pd_2)$ are interdependent. Knowing that the bond order is 0 in the excited state, it is very reasonable to believe that the $r(Pd_2)$ value would

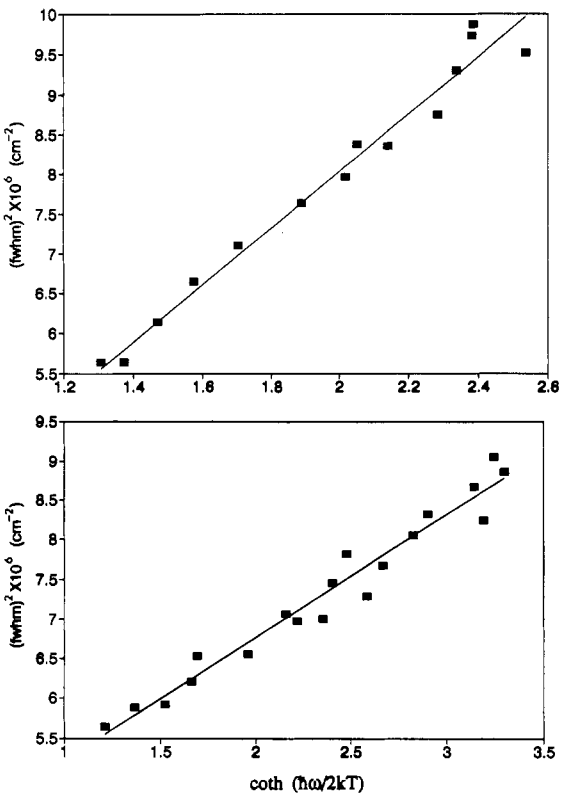

Figure 8. First-moment best fits $\bar{\nu}_{max}(d\sigma \rightarrow d\sigma^*)$ vs T for the $Pd_2(dmb)_2X_2$ complexes: top, X = Cl; bottom, X = Br. The square points are the experimental data; the line is the best fit.

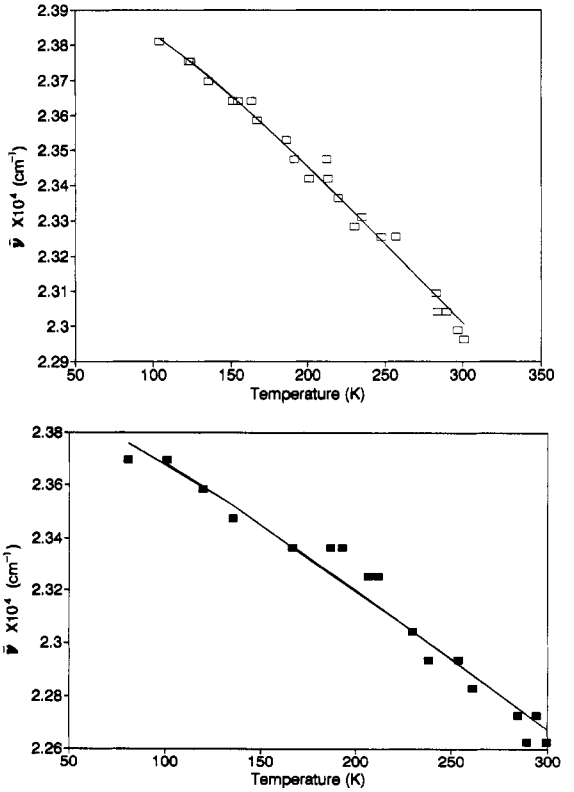

Figure 9. Second-moment best fits $(fwhm)^2$ vs $\coth(\hbar\omega_g/2kT)$) for the $Pd_2(dmb)_2X_2$ complexes: top, X = Cl; bottom, X = Br. The square points are the experimental data; the line is the best fit.

(41) (a) Harvey, P. D.; Gray, H. B. *J. Am. Chem. Soc.* **1988**, *110*, 2145. (b) Harvey, P. D.; Dallinger, R. F.; Woodruff, W. H.; Gray, H. B. *Inorg. Chem.* **1989**, *28*, 3057.

(42) Huang, K.; Rhys, A. *Proc. R. Soc., London* **1958**, *A204*, 406.

(43) This difference is not unusual. The lowest energy singlet and triplet Franck–Condon-active $\nu(Pt_2)$ values are found to be 145 and 150 cm^{-1}, respectively, for $Pt_2(POP)_4^{4-}$ (POP = $P_2O_5H_2^{2-}$): Stiegman, A. E.; Rice, S. F.; Gray, H. B.; Miskowski, V. M. *Inorg. Chem.* **1987**, *26*, 1112.

Table VI. Selected ΔQ Values vs $\hbar\omega_e(Pd_2)$ for $Pd_2(dmb)_2X_2$ (X = Cl, Br)[a,b]

Cl		Cl		Br		Br	
$\hbar\omega_e$/cm^{-1}	ΔQ/Å	$\hbar\omega_e$/cm^{-1}	ΔQ/Å	$\hbar\omega_e$/cm^{-1}	ΔQ/Å	$\hbar\omega_e$/cm^{-1}	ΔQ/Å
160	0.19	100	0.48	120	0.19	60	0.74
150	0.21	90	0.59	110	0.22	50	1.07
140	0.24	80	0.74	100	0.27	40	1.67
130	0.28	70	0.97	90	0.33		
120	0.33	60	1.32	80	0.42		
110	0.39	53	1.70	70	0.55		

[a] $\hbar\omega_g(Pd_2)$ for X = Cl, 174 cm^{-1}, and $\hbar\omega_g(Pd_2)$ for X = Br, 131 cm^{-1} (see Table I). [b] $\Delta Q = 4\pi(\hbar\omega_e(Pd_2))^2(\hbar(\hbar\omega_g(Pd_2))(A/c)\mu(\ln 2))^{1/2}$ where A is the slope of the graph (fwhm)^2 vs $\coth(0.72(\hbar\omega_g(Pd_2))/T)$.

range around 4.4 Å, a distance systematically encountered for the non-metal–metal-bonded d^8–d^8 $Pd_2(dmb)_2X_4$ complexes (X = Cl, I).[6,28] If this is the case, the ΔQ values would be around 1.68 Å and the computed $\hbar\omega_e(Pd_2)$ terms would take values of about 53 and 40 cm^{-1} for X = Cl and Br, respectively. These data are in the appropriate range for Pd_2 systems with very weak Pd···Pd interactions.[17b] Specifically, the $\hbar\omega(Pd_2)$ and $r(Pd_2)$ values are 19 and 30 cm^{-1} and 4.42 and 4.056 Å for [*cis*-$Pd(CNC(CH_3)_3)_2Cl_2]_2$, 32 cm^{-1} and 4.061 Å for [*cis*-$Pd(CN\text{-}2,6\text{-}(CH_3)_2C_6H_3)Cl_2]_2$, and 58 cm^{-1} and 3.593 Å for [*cis*-$Pd(CNC_6H_{11})_2Cl_2]_2$.[17b] In a more rigorous analysis, the comparison of the computed 53 and 40 cm^{-1} values for $\hbar\omega_e(Pd_2)$ (for X = Cl and Br, respectively) would not compare favorably with a 19 cm^{-1} value found for a distance of 4.4 Å! One must realize that the Huang–Rhys parameters (S)[42] would be very large ($S \sim 230$ for X = Cl and $\hbar\omega_e = 53$ cm^{-1}; $S \sim 169$ for X = Br and $\hbar\omega_e = 40$ cm^{-1}) and that the $\nu(M_2)$ modes generally possess some anharmonicities,[44] inducing large errors in the analysis for large S values.

The data for the dmb complexes make some sense in a physical way. The b and tmb ligands cannot accommodate M–M distances longer than ~3.3 Å,[38a] while the dmb ligand can bridge M atoms from 4.4[6,28] to 5.2 Å,[30] as already stated. The similarity in second-moment A values between $Pd_2(dmb)_2Cl_2$ and the unbridged $Mn_2(CO)_{10}$ is consistent with this model. Furthermore, the decrease in A upon going from X = Cl to X = Br appears to be a normal consequence of the lower $\nu(Pd_2)$ values in the Br derivatives (Table I), since $A = S(\hbar\omega_e)^2$ (assuming ΔQ to be a constant value). It is interesting to note that $\hbar\omega_g(Pd_2)^{Cl}/\hbar\omega_g(Pd_2)^{Br}$ is 1.328 and that $\hbar\omega_e(Pd_2)^{Cl}/\hbar\omega_e(Pd_2)^{Br}$ extracted from the A values assuming a same ΔQ (~1.68 ± 0.02 Å) is 1.325 also.

The second-moment B values (Table IV) are significantly smaller than those reported for $Rh_2b_4Cl_2^{2+}$, $Rh_2(TMB)_4Cl_2^{2+}$ and $Mn_2(CO)_{10}$,[39b] indicating that the Franck–Condon-active modes that are too energetic to contribute strongly to the temperature dependence are less important in the d^9–d^9 cases here. If such modes are ν(M–L), in particular ν(Pd–Cl), it appears reasonable to believe, since the Cl atomic contributions to the HOMO and LUMO are 4–10% in both cases (Table II), that the relative intensity of such a vibrational progression would not be a dominant one. Similarly, the fact that such modes (ν(Pd–C)) could also be potential candidates to make the B values non-zero in these cases.

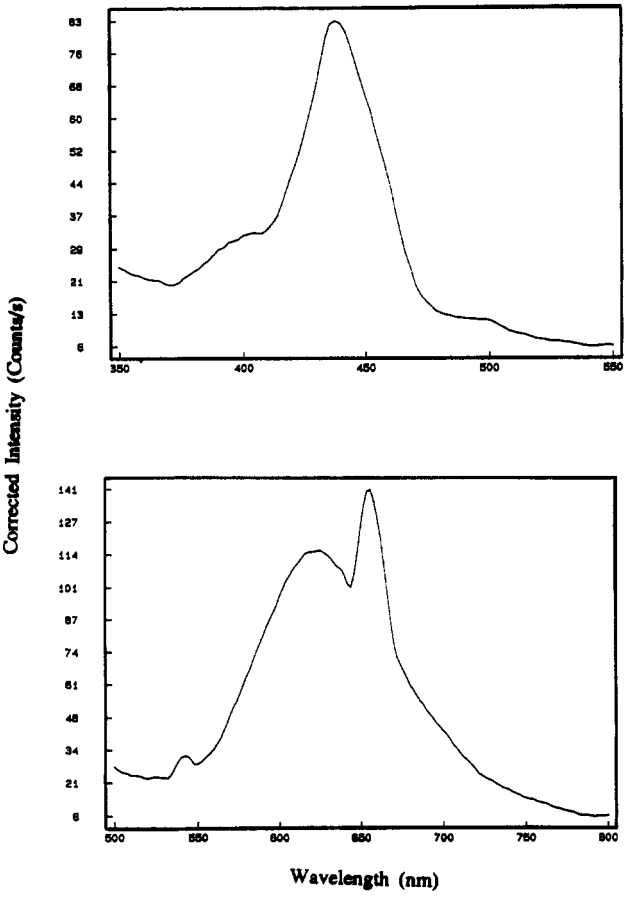

Figure 10. Emission (bottom) and excitation (top) spectra of $Pd_2(dmb)_2Cl_2$ in butyronitrile glasses at 77 K: top, emission wavelength = 625 nm; bottom, excitation wavelength = 438 nm. Peaks at ~545 and ~655 nm are instrumental artifacts.

No analysis has been performed for the related compounds $Pd_2(tmb)_2X_2$ (X = Cl, Br), but it is strongly anticipated that similar results will be obtained.

Excited-State Properties. Organometallic complexes do not have the reputation for being intense emitters,[45] but both d^8–d^8 and d^{10}–d^{10} complexes of Pd and Pt are known to be relatively strongly luminescent (regardless of the nature of the ligand).[41,46] The d^9–d^9 species (particularly for dppm complexes) are found to be either nonemissive (M = Pd) or weakly luminescent (M = Pt).[25] We have been able to detect some weak luminescence ($\Phi < 0.001$) for $Pd_2(dmb)_2X_2$ complexes (X = Cl, Br) in 77 K glasses, in the 600–700-nm range (Figures 10 and 11).[47] The excitation spectra superimpose on the absorption spectra, which indicates that the observed emissions do not arise from impurities. The emission lifetimes (τ_e) measured at 77 K in MeOH/EtOH mixtures (1:1) are found to be relatively short (from 70 to 180 ns; see Table VII) and are consistent with the weak observed intensity. Since the Stokes shifts range from ~7000 to 8500 cm^{-1} (for the dmb complexes, for instance), these emissions must arise from the low-energy (short-lived) triplet states. For comparison purposes, the τ_e values for the tmb complexes have been obtained and compare favorably to those obtained for the dmb ones. The τ_e value for X = Cl is smaller than that for X = Br, appearing to contradict what would be expected for a normal

(44) (a) Some anharmonicity constants (x_{11}cm^{-1}) have been evaluated for binuclear complexes via resonance Raman spectroscopy: $[Mo_2Cl_8]^{-4}$, $\nu(Mo_2)$ = 339.6 cm^{-1}, x_{11} = –0.76 cm^{-1};[44b] $[Mo_2Br_8]^{4-}$, $\nu(Mo_2)$ = 336.9 cm^{-1}, x_{11} = –0.48 cm^{-1},[44c] $[Re_2Cl_8]^{2-}$, $\nu(Re_2)$ = 272.6 cm^{-1}, x_{11} = –0.48 cm^{-1},[44c] $[Re_2Cl_8]^{2-}$, $\nu(Re_2)$ = 272.6 cm^{-1}, x_{11} = –0.35 cm^{-1}; $[Re_2Cl_8]_2$ = 276.2 cm^{-1}, x_{11} = –0.39 cm^{-1},[44d] $Ru_2(O_2CCH_3)_4Cl$, $\nu(Ru_2)$ = 327.6 cm^{-1}, x_{11} = –0.13 cm^{-1}; $Ru_2(O_2CC_3H_7)_4Cl$, $\nu(Ru_2)$ = 331.4 cm^{-1}, x_{11} = –0.27 cm^{-1}.[44e]. (b) Clark, R. J. H.; Franks, M. L. *J. Am. Chem. Soc.* **1975**, *97*, 2691. (c) Clark, R. J. H.; D'Urso, N. R. *J. Am. Chem. Soc.* **1978**, *100*, 3088. (d) Clark, R. J. H.; Franks, M. L. *J. Am. Chem. Soc.* **1976**, *98*, 2763. (e) Clark, R. J. H.; Franks, M. L. *J. Chem. Soc., Dalton Trans.* **1976**, 1825. (f) For samll $\nu(M_2)$ values, x_{11} are expected to be small as well. For instance, the $^{133}Cs_2$ dimer (a relevant example for this work) exhibits an $r(Cs_2)$ value of 4.47 Å with $\nu(Cs_2)$ = 42.022 cm^{-1} and x_{11} = 0.0823 cm^{-1}.[44g] (g) Huber, K. P.; Herzberg, G. *Constants of Diatomic Molecules*; Van Nostrand: New York, 1979.

(45) Lees, A. J. *Chem. Rev.* **1987**, *87*, 711.

(46) (a) Harvey, P. D.; Adar, F.; Gray, H. B. *J. Am. Chem. Soc.* **1989**, *111*, 1312. (b) Harvey, P. D.; Gray, H. B. *Polyhedron* **1990**, *9*, 1949. (c) Fordyce, W. A.; Brummer, J. G.; Crosby, G. A.; *J. Am. Chem. Soc.* **1981**, *103*, 7061.

(47) We find that the relative emission intensities depend upon the solvent for the same substrate concentration. On some occasions, the emission was not detected. This observation is consistent with the fact that the emission lifetimes and λ_{max} for $Pt_2(dppm)_2Cl_2$ greatly depend upon the solvent of crystallization.[25a]

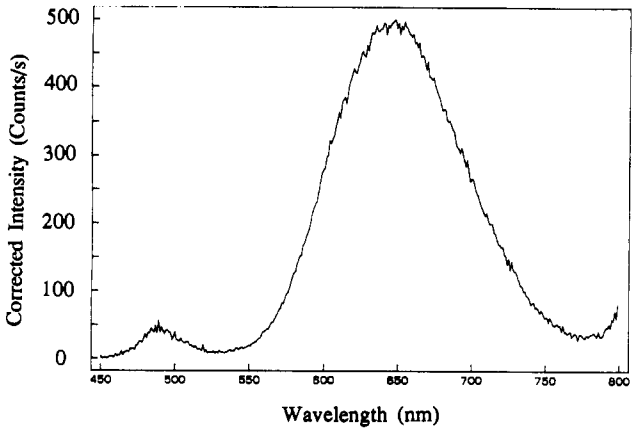

Figure 11. Emission spectrum of $Pd_2(dmb)_2Br_2$ in an ethanol glass at 77 K. Excitation wavelength = 420 nm. The emission band located at ~440 nm is due to an impurity.

Table VII. Emission Spectroscopic and Lifetime Data at 77 K

	λ_{max}/nm[a]	τ_e/ns[b]		λ_{max}/nm[a]	τ_e/ns[b]
$Pd_2(dmb)_2Cl_2$	625 ± 5	71 ± 6	$Pd_2(tmb)_2Cl_2$		81 ± 15
$Pd_2(dmb)_2Br_2$	650 ± 5	177 ± 34	$Pd_2(tmb)_2Br_2$		125 ± 16

[a] In ethanol glass. [b] In a 1:1 methanol/ethanol mixture.

heavy-atom effect. It is therefore believed that the Pd–Cl bond is more photolabile than the Pd–Br one.

The excited-state driving forces for electron transfers ($E^{*/+}$) have been evaluated using cyclic voltammetry and emission spectroscopy. The d^9–d^9 $Pd_2(dppm)_2X_2$ complexes (X = Cl, Br, I) exhibit redox potentials of +0.98, +0.84, and +0.70 V vs SCE for a one-electron oxidation and −1.26, −1.23, and −1.15 V vs SCE for a two-electron reduction for X = Cl, Br, and I, respectively.[48] We have measured the one-electron oxidation potentials (by cyclic voltammetry using acetonitrile as solvent); they are located at +0.78 and +0.64 V vs SCE for X = Cl and Br, respectively, as quasi-reversible waves. These data compare favorably with those for the dppm analogue.[49] The $E^{*/+}$ values are then easily extracted ($E^{(triplet} - E^{*/+}$) for both the chloride, 1.20 V, and bromide complexes, 1.27 V, vs SCE. These potentials are great but not great enough to reduce halocarbons such as $CHCl_3$ and CH_2Cl_2, for which reduction potentials are greater than −2 V vs SCE. This observation represents a very serious argument in favor of the photoinduced atom-transfer reactivity of the $Pd_2(dmb)_2X_2$ complexes (X = Cl, Br) toward halocarbons.[6] No reduction wave was observed in the −1.5 to 0 V vs SCE range.

The picosecond flash photolysis spectra (see Figure 12 as a typical example) are characterized by a bleached band (OD ~ −0.17 for a solution made up with an original OD or ~0.50) at ~420 nm ($d\sigma \rightarrow d\sigma^*$) and the appearance of a weak (+0.058 OD) and broad transient band located at ~620 nm. The excited lifetimes are less than 30 ps, like those for $Rh_2b_4Cl_2^{2+}$ [38a] and $Mn_2(CO)_{10}$.[50] The signals remain invariant up to a few nanoseconds. Similar flash photolysis experiments performed on Pd_2-

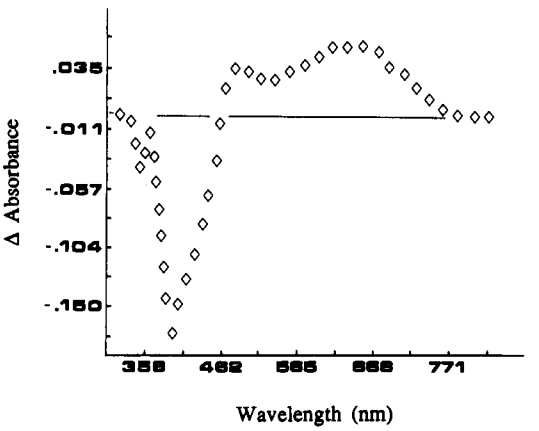

Figure 12. Picosecond flash photolysis spectrum of $Pd_2(dmb)_2Br_2$ in acetonitrile. Delay time = 30 ps; λ_{exc} = 355 nm.

$(CNCH_3)_6^{2+}$ produce a transient species located at ~405 nm (associated with a narrow and intense band ϵ_{405} = 50 000 M^{-1} cm^{-1}) which has been identified to be the mononuclear $Pd(CNCH_3)_3^{+}$ complex.[1b] The rate of recombination ($2Pd(CNCH_3)_3^{+} \xrightarrow{k} Pd_2(CNCH_3)_6^{2+}$) is near the diffusion-controlled limit (1×10^9 M^{-1} s^{-1}).[1b] In the case of the $Pd_2(dmb)_2X_2$ complexes (X = Cl, Br), the recombination pathway is monomolecular (first-order) and the rate of recombination would appear to be larger than 3.33×10^{10} s^{-1}. While the energy gaps between the $d\sigma \rightarrow d\sigma^*$ absorption and the transient maxima of the $Pd_2(CNCH_3)_6^{2+}$ (~7700 cm^{-1}) and $Pd_2(dmb)_2X_2$ compounds (~8400 cm^{-1} for X = Cl, Br) compare favorably, the shape and ϵ do not. It is known that the efficient deactivation pathway of the excited states of singly metal–metal-bonded complexes is the characteristic homolytic metal–metal bond scission.[50,51] In principle, for the bridged metal–metal-bonded species, no net photoproduct should result from this metal–metal dissociative process. But, during our flash photolysis experiments, some slow photoinduced disappearance of the d^9–d^9 materials were observed, was the yellow solutions were slowly turning to colorless ones. The $Rh_2b_4X_2^{2+}$ and $Rh_2(TMB)_4X_2^{2+}$ complexes (X = Cl, Br) are known to undergo photoinduced homolytic Rh–X bond cleavages in the excited state, which lead to the eventual formation of the d^8–d^8 reduced species $Rh_2b_4^{2+}$ and $Rh_2(TMB)_4^{2+}$.[38a] We did not attempt to identify the photoproducts in our experiments, but we come to the conclusion that both photoinduced homolytic Pd–Pd (with rapid recombination) and Pd–X bond scissions (slowly leading to products) must be considered as the two excited-state-deactivation pathways. The hypothesis for a photoinduced-Pd–X bond scission is supported by the fact we observe τ_e(X = Cl) < τ_e(X = Br).

Acknowledgment. This research was supported by the NSERC and FCAR. P.D.H. thanks Dr. S. Hubig (Center for Fast Kinetics), Mr. D. Piché (Université de Sherbrooke), and Mr. Scott Cummings (University of Rochester) for technical assistance in the measurements of the picosecond flash photolysis spectra, the PC-MODEL computations, and emission lifetime measurements, respectively.

Supplementary Material Available: A plot of the UV–visible frequencies of $Pd_2(dmb)_2I_2$ vs T, a plot of $\bar{\nu}(d\sigma \rightarrow d\sigma^*)$ vs T for $Pd_2(dmb)_2I_2$, and a PC-MODEL structure for $Pd_2(H)_4(C_{14}H_{18})_2Cl_2$ (4 pages). Ordering information is given on any current masthead page.

(48) Nembra, G.; Lemoine, P.; Braustein, P.; Debellefon, C. D.; Ries, M. *J. Organomet. Chem.* **1986**, *304*, 245.

(49) (a) We have also measured $E^{0/+}$ for $Pd_2(dmb)_2I_2$ (+0.38 V vs SCE). The $Pd_2(dmb)_2I_2$ species have been generated by the conventional excess addition of KI to a solution of $Pd_2(dmb)_2Cl_2$.[49b] By cyclic voltammetry, the peak located at +0.78 V disappears and a new one appears at +0.38 V vs SCE. By UV–vis spectroscopy, the addition produces a new spectrum, dominated by two intense bands (~450 and 350 nm). The temperature dependence of $\bar{\nu}_{max}$ showed the common blue shift (first-moment A = −530 cm^{-1}, B = 24,400 cm^{-1}, and $\hbar\omega_l$ = 100 cm^{-1}) and a decrease in fwhm for the low-energy band, upon cooling. The second band (350 nm) was not temperature dependent. No attempt to isolate the product in the pure state has been made. The data are available in the supplementary material. (b) Kullberg, M. L.; Kubiak, C. P. *Organometallics* **1984**, *3*, 632.

(50) (a) Freedman, A.; Bersohn, R. *J. Am. Chem. Soc.* **1978**, *100*, 4116. (b) Rothberg, L. J.; Cooper, N. J.; Peters, K. S.; Vaida, V. *J. Am. Chem. Soc.* **1982**, *104*, 3536.

(51) (a) Wrighton, M. S.; Ginley, D. S. *J. Am. Chem. Soc.* **1975**, *97*, 2065. (b) Reinking, M. K.; Kullberg, M. L.; Cutler, A. R.; Kubiak, C. P. *J. Am. Chem. Soc.* **1985**, *107*, 3517. (c) Hughey, J. L.; Anderson, C. P.; Meyer, T. J. *J. Organomet. Chem.* **1977**, *125*, C49. (d) See also: Meyer, T. J.; Caspar, J. V. *Chem. Rev.* **1985**, *85*, 187.